

Dynamic Phases, Pinning, and Pattern Formation for Driven Dislocation Assemblies

C. Zhou, C. Reichhardt, C.J. Olson Reichhardt, and I.J. Beyerlein

*Center for Nonlinear Studies and Theoretical Division,
Los Alamos National Laboratory, Los Alamos, New Mexico 87545, USA*

(Dated: July 31, 2012)

We show that driven dislocation assemblies exhibit a set of dynamical phases remarkably similar to those of driven systems with quenched disorder such as vortices in superconductors, magnetic domain walls, and charge density wave materials. These phases include jammed, fluctuating, and dynamically ordered states, and each produces distinct dislocation patterns as well as specific features in the noise fluctuations and transport properties. Our work suggests that many of the results established for systems with quenched disorder undergoing depinning transitions can be applied to dislocation systems, providing a new approach for understanding dislocation pattern formation and dynamics.

PACS numbers: 74.20.Mn, 74.72.-h, 71.45.Lr, 74.50.+r

There are numerous examples of systems of collectively interacting particles that, when driven externally, depin and undergo dynamical pattern formation and/or dynamic phase transitions, such as a transition from a fluctuating to a nonfluctuating state. Such systems include domain walls, driven vortices in type-II superconductors [1–6], sliding charge density waves [7], and driven Wigner crystals [8]. In these systems, fluctuating and intermittent dynamics arise just above depinning when an applied external force is increased from zero, while for higher drives the particles dynamically order into patterns such as anisotropic crystals or moving smectic phases with different types of fluctuation statistics [9–13]. Dislocations in materials are known to undergo a transition at the onset of irreversibility or yielding that has similarities to depinning [14, 15]; however, it has not been shown whether driven dislocations can exhibit the same general features as other systems with depinning transitions. Establishing such a connection could potentially open an entirely new paradigm for understanding driven dislocations.

It is known that organized dislocation structures within individual crystals, such as tangles, cells, or planar walls, can become more refined and better defined as stress or strain increases. Two-dimensional (2D) and three-dimensional (3D) dislocation dynamics simulations based on linear elasticity theory predict self-organization of dislocation assemblies into varying configurations, such as pileups near the yielding or depinning transition [14–16] and 2D mobile walls [17, 18] or 3D slip bands [19, 20] under an external drive. Below a critical stress where dislocations show no net motion, the system is considered jammed [21, 22], while intermittent or strongly fluctuating behavior with highly jerky or avalanche-like motion occurs above the critical stress [17]. Avalanche behavior with power-law velocity distributions is proposed to be a signature of critical dynamics [17, 18, 23, 24]. No correlations between the transitions in patterning and the intensity of applied stress or strain have been established before now. Here we demonstrate that driven

dislocation assemblies exhibit the same nonequilibrium phases observed for collectively interacting particle systems exhibiting depinning, including pattern organization in the pinned state, a strongly fluctuating intermittent phase with a coexistence of pinned and moving particles [1, 3, 10, 25, 26], and at higher drive, when the effectiveness of the substrate is reduced, a phase in which the dislocations organize into moving wall structures [2–4, 6, 7, 11–13]. The onsets of these different dynamical regimes are correlated with pronounced changes in the transport curves [1, 5], noise properties [3, 27], and spatial structures [4, 6, 9]. The onset of these phases can be observed via changes in the dislocation structure, mobility, velocity distribution, and velocity noise. Our work implies that many of the established results obtained for driven vortex and other systems can be used to understand dislocation dynamics.

We utilize a discrete dislocation dynamics model with periodic boundary conditions for a 2D cross section of a sample containing $N_D = 480$ straight edge dislocations that glide along parallel slip planes. This model was previously shown to capture the behavior observed in stressed anisotropic materials, particularly the intermittent flow near the onset of motion [17, 21, 22]. An equal number of positive and negative moving dislocations are randomly placed in the sample and can move in the positive or negative x -direction depending on the sign of their Burgers vector \mathbf{b} . At most one dislocation is allowed to reside on a plane, so in-plane pile-ups are prevented. The dislocations are also restricted from leaving their assigned glide plane. Rather than imposing an annihilation rule [15, 17, 18], we enforce that two adjacent glide planes must be separated by at least δy , where δy is on the order of the Burgers vector of the dislocations [21, 22, 30].

The dislocations interact via a long-range anisotropic stress field that is attractive between two oppositely signed dislocations and repulsive for like-signed pairs. We utilize a replicated image model to allow a large num-

ber of dislocations to be simulated efficiently over long times [31]. Within the simulation volume, all dislocations are subject to the stress fields of all surrounding dislocations regardless of their position. To best make the connection with particle systems, nucleation of fresh dislocations during loading is suppressed. Under an external applied stress τ_{ext} , dislocation i moves along x in its assigned plane according to an overdamped equation of motion given by $\eta \frac{dx_i}{dt} = b_i \left(\sum_{j \neq i}^N \tau_{\text{int}}(\mathbf{r}_j - \mathbf{r}_i) - \tau_{\text{ext}} \right)$ where x_i is the x coordinate of dislocation i at point $\mathbf{r}_i = (x_i, y_i)$ with Burgers vector value b_i , η is the effective friction, and $\tau_{\text{int}}(\mathbf{r}_j - \mathbf{r}_i)$ is the long-range shear stress on dislocation i generated by dislocation j . The external load on a dislocation is proportional to the stress, $F_d = b\tau_{\text{ext}}$. For $\mathbf{r} = (x, y) = (x_j, y_j) - (x_i, y_i)$, $\tau_{\text{int}}(\mathbf{r}_j - \mathbf{r}_i)$ for an edge dislocation with Burgers vector value b is $\tau_{\text{int}}(\mathbf{r}) = b\mu[x(x^2 - y^2)]/[2\pi(1 - \nu)(x^2 + y^2)^2]$ where μ is the shear modulus and ν is the Poisson's ratio. The length of the square simulation cell L is set to unity and the simulation volume remains fixed throughout loading. We normalize our units such that $b = 1$, $\eta = 1$, and $\mu/2\pi(1 - \nu) = 1$. The system is initially allowed to relax without an applied external drive. After relaxation, the external drive is applied quasi-statically, with sufficiently long waiting times between increments to avoid transient effects. We measure the average absolute value of the dislocation velocities $\langle |v| \rangle$ as a function of the stress. This is analogous to the voltage versus applied current curve for vortices in superconductors.

In order to detect and characterize the dislocation content and charge of the wall structures, we examine the distribution of $d_x = |x_i - x_j|$, the x -axis separation between two dislocations lying on adjacent planes. The fraction of dislocation pairs with $d_x < w$ is denoted as $P^w = n_{d_x < w}/n_{\text{tot}}$, where w is the pre-assigned maximum wall width, n_{tot} is the total number of pairs in this system, and $n_{d_x < w}$ is the number of pairs satisfying $d_x < w$. Here we set $w = 0.05$, although other reasonable values, such as $w = 0.02$, give qualitatively similar results. To distinguish unipolar from dipolar walls, we discriminate between those pairs of like and unlike sign that lie within the critical wall width. The difference $B = P_{++,-} - P_{+-}$ between the fraction of pairs of like (unlike) sign $P_{++,-}$ (P_{+-}) is directly related to the net Burgers vector around one dislocation within the wall width w . Thus, when a dipolar wall forms, B approaches zero since the number of unlike sign pairs is almost the same as the number of like sign pairs. When a unipolar wall forms, P_{+-} is zero and B is equal to $P_{++,-}$.

As the system of randomly positioned dislocations is allowed to relax under zero applied stress, the dislocations reassemble into a locked configuration determined by the long-range stress fields they collectively produce. The relaxed arrangement of the dislocations shown in Figure 1(a) is disordered and contains no percolating

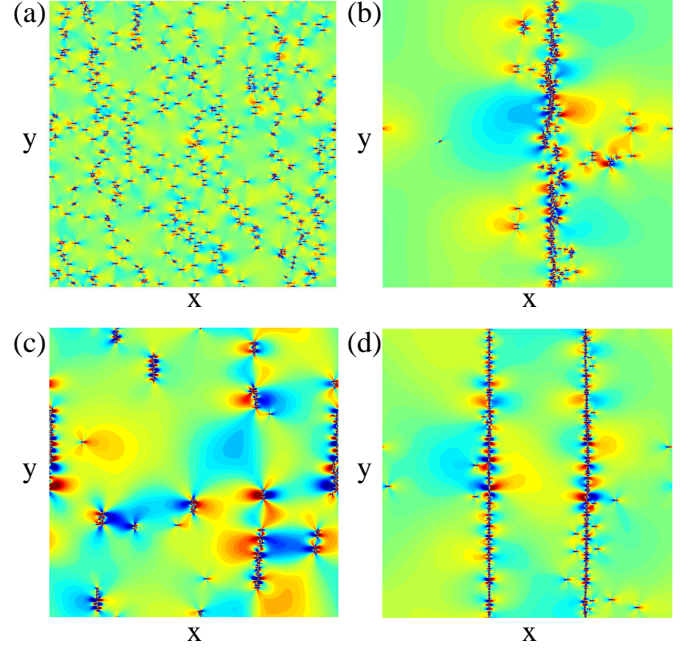


FIG. 1: Stress maps of the sample range from large negative (blue) to large positive (red) stress. (a) The initial dislocation positions at zero load. (b) Just before yielding, the dislocations are predominantly located at pile-ups to form a single bipolar wall. (c) Above yielding at $F_d = 3.6$, the wall breaks apart and the structure exhibits intermittent dynamics. (d) At $F_d = 8.0$ there is a dynamical ordering into polarized walls, each composed of dislocations with the same Burgers vector orientation.

walls. The internal stresses generated by this spatially random arrangement are high and are distributed uniformly across the volume.

For loads $0 < F_d < 2.0$, the dislocation pattern slowly changes after each load increment but $\langle |v| \rangle$ goes to zero in the long time limit, indicating that the system is in the jammed phase below the critical yield [21, 22]. Under these low drives, any dislocation motion merely causes the dislocations to lock into another immobilized pattern. Figure 1(b) illustrates a typical locked dislocation configuration for loads just below critical yield (i.e., $F_d < F_c$), where most dislocations have assembled into a dipolar wall comprised of a disordered arrangement of positive and negative dislocations that cannot move past one another. Compared to the initial state [Fig. 1(a)], the internal stress [Fig. 1(b)] remains high but is more localized, and large stress concentrations appear in the vicinity of the wall. Such walls are analogous to the model of a “polarized” wall [32, 33], with dislocations of predominantly one sign on one side of the wall and the other sign on the other side. They are thought to be responsible for the observed hysteresis in unloading or the Bauschinger effect in subsequent reverse loadings [34, 35]. Observations of polarized walls have been reported in crystals deformed

to large strains [36–38].

Just above yielding, the dipolar wall structure breaks down as shown in Fig. 1(c) and the system enters a state characterized by strong fluctuations in the dislocation positions. The dipolar walls repeatedly break up and reform, while the remaining wall fragments become smaller at higher drives and show continual change. The fluctuating state persists up to $F_d = 5.0$, when a new type of dynamic pattern appears where the dislocations form unipolar walls composed of only one type of dislocation, either negative or positive, as shown in Fig. 1(d). These walls can be identified as disordered tilt walls. An ideal model of a tilt wall involves a periodic array of edge dislocations that accommodate a tilt misorientation between two adjoining crystals. The development of low-misoriented tilt walls is suspected to be a precursor for the eventual formation of subgrains in heavily deformed crystals [39, 40]. Most importantly, when the unipolar walls form, the internal stress decreases in extent and intensity. The alternating positive and negative stress pattern that develops along the wall in Fig. 1(d) is consistent with the theoretical prediction for an infinite array of perfectly aligned, like-signed edge dislocations [41] from linear elasticity theory. Thus, the high applied drive enables the dislocations to assemble into a low energy ordered structure, a result that is consistent with the theories of substructure development proposed by Kuhlman-Wilsdorf [33].

In Fig. 2 we show that the changes in the dislocation structure produce signatures in $\langle |v| \rangle$ versus F_d for the system in Fig. 1. The upper curve in Fig. 2(b) shows the simple linear dependence of $\langle |v| \rangle$ on F_d expected for a single dislocation. For the interacting system, $\langle |v| \rangle$ is zero below yielding for $0.0 < F_d < 2.0$, increases nonlinearly for $2.0 \leq F_d < 7.5$, and then starts to become linear again for $F_d \geq 7.5$. Figure 2(a) characterizes the ordering dynamics as a function of F_d . Since the system is initialized in a random state containing no walls, $P_{+-} \approx 0$ at $F_d = 0$, but as the load increases, P_{+-} reaches a maximum just below the yielding point as shown in Fig. 1(b) where a large dipolar wall forms. Above yielding, P_{+-} decreases in the fluctuating regime when the walls break up, and it gradually drops to zero in the high-driving region where the unipolar walls form. To identify the formation of the unipolar dislocation walls, we measure $P_{++,-,-}$, which rises for $F_d > 5.0$ in Fig. 2(a). Also shown in Fig. 2(a) is the net Burgers vector of the walls, indicating that for $F_d > 5.0$ the walls are indeed unipolar and contain either exclusively positive or negative dislocations. Samples with smaller numbers of dislocations show the same general features in P_{+-} , $P_{++,-,-}$, and their difference B , as shown in Suppl. Fig. 1 [42].

The overall dynamics illustrated in Fig. 1 and Fig. 2 are remarkably similar to those observed in driven systems with quenched disorder. For example, for vortex matter as a function of external drive, there is a low

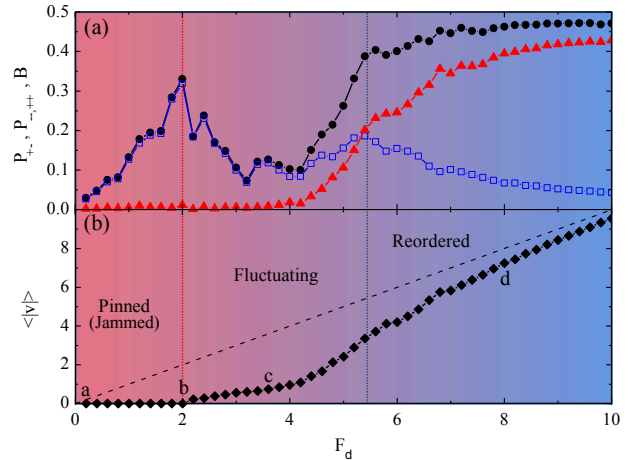


FIG. 2: (a) P_{+-} (blue squares), the fraction of dipolar walls, vs F_d has a peak just below yielding. $P_{++,-,-}$ (black circles), the fraction of uni-polar walls, passes through a plateau when the polarized wall state forms. B (red triangles) is a measure of the net Burgers vector in the walls. (b) The average absolute value of the dislocation velocity $\langle |v| \rangle$ (solid lower curve) vs F_d . The upper dashed curve shows $\langle |v| \rangle$ for non-interacting dislocations. Visible in the lower curve is a yielding point, a nonlinear region corresponding to the disordered or fluctuating regime, and a linear region at high drives when the system is dynamically ordered. Points a, b, c, and d indicate the F_d values illustrated in Fig. 1.

drive pinned phase, a strongly fluctuating phase where the vortex lattice structure is disordered, and a highly driven phase where dynamical pattern formation occurs [2, 3, 13]. The corresponding vortex velocity-force curves also show the same features: the fluctuating phase is correlated with a nonlinear region, while in the dynamically reordered phase the velocity depends linearly on the drive [1, 3, 5, 10].

The dynamical phases in the vortex system have also been characterized by changes in the velocity noise fluctuations across different regimes. Just above depinning in the fluctuating regime, there is a strong $1/f^\alpha$ noise signal [1, 3] associated with a bimodal velocity distribution that indicates a coexistence of pinned and moving vortices [3, 10, 43]. The onset of dynamical ordering is accompanied by a drop in the noise power S_0 as well as the appearance of narrow band noise features [3, 27]. For the dislocation system, in Fig. 3(a) we plot the instantaneous velocity distribution $P(|v|)$ in the fluctuating phase at $F_d = 3.2$. We find a bimodal velocity distribution that appears because a portion of the dislocations are immobilized in pileups while other dislocations have broken out of pileups and are mobile. A similar bimodal velocity distribution appears in the fluctuating phase for driven vortices and colloids. The corresponding power spectrum $S(f)$ presented in Fig. 3(b) of the time series of the average dislocation velocity has a $1/f^{1.5}$ signal in

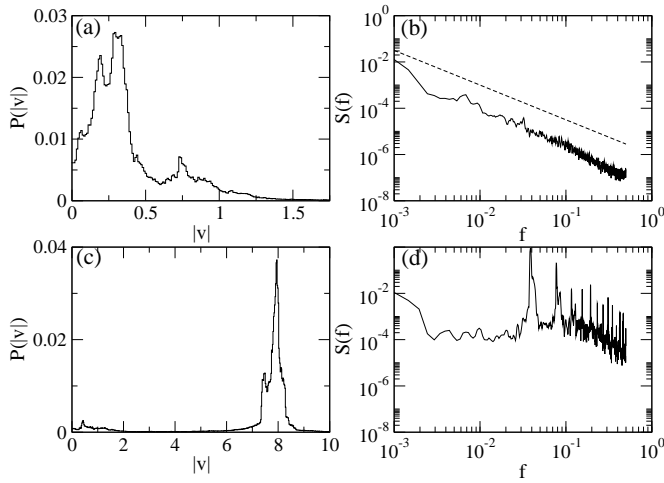


FIG. 3: (a) $P(|v|)$ at $F_d = 3.2$ is bimodal in the fluctuating phase. (b) The corresponding $S(f)$ from the time series of the velocity has a $1/f^{1.5}$ shape. (c) $P(|v|)$ for $F_d = 8.0$ in the ordered phase shows a sharp peak. (d) The corresponding $S(f)$ has a characteristic peak indicating narrow band noise.

this regime, in good agreement with studies of driven vortices. At $F_d = 8.0$ [Fig. 3(c)] in the dynamically ordered phase, $P(|v|)$ has a single sharp peak and the corresponding $S(f)$ in Fig. 3(d) has a narrow band feature with a characteristic frequency generated by the formation of an ordered structure of unipolar walls. In Fig. 4(a) the noise power S_0 for a fixed frequency reaches a peak in the middle of the fluctuating disordered phase and then decreases as the dynamically ordered phase of unipolar walls is approached.

By conducting a series of simulations for varied dislocation densities, $\rho = N_D/L^2$, and analyzing the ordering dynamics, we construct the dynamic phase diagram shown in Fig. 4(b). The lower curve indicates the yielding transition from the low drive jammed or pinned phase of dipolar walls to the fluctuating disordered phase. The onset of the dynamically ordered phase is defined as the force at which the unipolar wall structures start to form, and is plotted in the upper curve. As ρ increases, the yielding point rises to higher F_d since the dislocations have a more difficult time breaking through the dipolar walls that form. The increase in yield threshold with increasing ρ remains robust when we perform simulations with different initial dislocation configurations. Fig. 4(b) shows that the onset of the high drive dynamically ordered phase also increases in a similar fashion with increasing ρ . This phase diagram exhibits the same features observed for vortex systems as a function of pinning strength vs external drive, where both the critical depinning force and the onset of the ordering rise to higher drives with increasing pinning strength [13]. For the dislocation system, increasing ρ is equivalent to increasing the pinning strength. In our simulation, the pin-

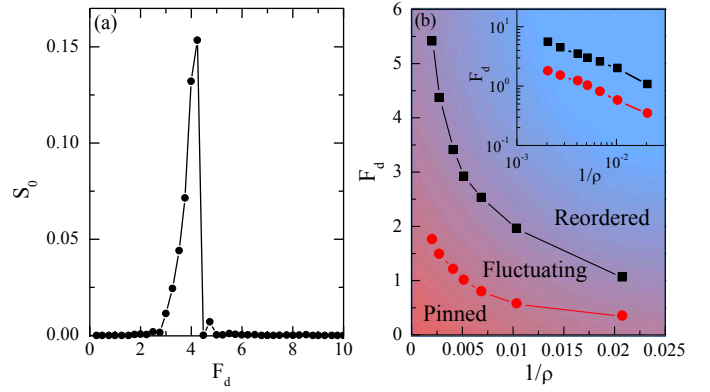


FIG. 4: (a) S_0 vs F_d at a fixed frequency of $f = 5 \times 10^{-3}$ has a peak in the fluctuating phase and drops as the dynamically ordered phase is approached. (b) The dynamical phase diagram F_d vs $1/\rho$, where ρ is the dislocation density. The lower curve (red circles) indicates the onset of yielding and the upper curve (black squares) is the onset of the dynamically induced ordered phase; the fluctuating phase falls between the two curves. Both the critical yielding and the dynamical ordering shift to higher drives as the ρ increases. Inset: The same curves plotted on a log-log scale.

ning strength is directly related to the dislocation dipole break stress given by $\mu/(8\pi\gamma(1-\nu))$ [45], where $\gamma \propto 1/\rho$. Thus, as Fig. 4(b) shows, the pinning strength scales as ρ . This differs from the recent simulation results obtained in smaller systems [21, 22].

The type of ordered state that forms in the strong driving regime varies depending on the rate at which the external load is applied. The ordered polarized walls illustrated in Fig. 1 form under continuous sweeps of the load. If the load is instead instantaneously set to a high value, we observe a transient disordered phase followed by the formation of multiple lower density unipolar walls, as illustrated in Suppl. Fig. 2 [42], instead of the two unipolar walls shown in Fig. 1(d). As for the nature of the yielding transition, recent work on depinning systems has suggested that plastic depinning falls into the class of absorbing phase transitions, specifically directed percolation [25, 29], suggesting that the onset of yielding for dislocation systems could also fall into the class of directed percolation.

In summary, we have shown that driven dislocation assemblies exhibit the same nonequilibrium phases observed for systems of collectively interacting particles such as vortices in disordered superconductors. These include a jammed phase analogous to a pinned state, a fluctuating or disordered phase, and dynamically ordered or pattern forming states. All of the states are associated with transport signatures such as changes in the transport noise fluctuations as well as features in the dislocation velocity vs applied shear, in analogy with velocity-force curves.

We acknowledge helpful discussions with Karen Dah-

men. This work was carried out under the auspices of the NNSA of the US DoE at LANL under Contract No. DE-AC52-06NA25396.

-
- [1] S. Bhattacharya and M.J. Higgins, Phys. Rev. Lett. **70**, 2617 (1993).
 - [2] A.E. Koshelev and V.M. Vinokur, Phys. Rev. Lett. **73**, 3580 (1994).
 - [3] C.J. Olson, C. Reichhardt, and F. Nori, Phys. Rev. B **81**, 3757 (1998).
 - [4] F. Pardo, F. de la Cruz, P. Gammel, E. Bucher, and D.J. Bishop, Nature (London) **396**, 348 (1998).
 - [5] M.C. Hellerqvist, D. Ephron, W.R. White, M.R. Beasley, and A. Kapitulnik, Phys. Rev. Lett. **76**, 4022 (1996).
 - [6] A.M. Troyanovski, J. Aarts, and P.H. Kes, Nature (London) **399**, 665 (1999).
 - [7] R. Danneau, A. Ayari, D. Rideau, H. Requardt, J.E. Lorenzo, L. Ortega, P. Monceau, R. Currat, and G. Grübel, Phys. Rev. Lett. **89**, 106404 (2002).
 - [8] C. Reichhardt, C.J. Olson, N.J. Grønbech-Jensen, and F. Nori, Phys. Rev. Lett. **86**, 4354 (2001).
 - [9] U. Yaron *et al.*, Nature (London) **376**, 753 (1995) Structural evidence for a two-step process in the depinning of the superconducting flux-line lattice. *Nature (London)* 376:753-755.
 - [10] M.C. Faleski, M.C. Marchetti, and A.A. Middleton, Phys. Rev. B **54**, 12427 (1996).
 - [11] L. Balents, M.C. Marchetti, and L. Radzihovsky, Phys. Rev. B **57**, 7705 (1998).
 - [12] P. Le Doussal and T. Giamarchi, Phys. Rev. B **57**, 11356 (1998).
 - [13] K. Moon, R.T. Scalettar, and G.T. Zimányi, Phys. Rev. Lett. **77**, 2778 (1996).
 - [14] P. Moretti, M.-C. Miguel, M. Zaiser, and S. Zapperi, Phys. Rev. B **69**, 214103 (2004).
 - [15] L. Laurson, M.-C. Miguel, and M.J. Alava, Phys. Rev. Lett. **105**, 015501 (2010).
 - [16] B. Bakó, D. Weygand, M. Samaras, W. Hoffelner, and M. Zaiser, Phys. Rev. B **78**, 144104 (2008).
 - [17] M.-C. Miguel, A. Vespignani, S. Zapperi, J. Weiss, and J.R. Grasso, Nature (London) **410**, 667 (2001).
 - [18] M.-C. Miguel, A. Vespignani, M. Zaiser, and S. Zapperi, Phys. Rev. Lett. **89**, 165501 (2002).
 - [19] F.F. Csikor, C. Motz, D. Weygand, M. Zaiser, and S. Zapperi, Science **318**, 251 (2007).
 - [20] Z.Q. Wang, I.J. Beyerlein, and R. LeSar, Phil. Mag. **88**, 1321 (2008).
 - [21] G. Tsekenis, N. Goldenfeld, and K.A. Dahmen, Phys. Rev. Lett. **106**, 105501 (2011).
 - [22] I. Groma, G. Györgyi, and P.D. Ispanovity, Phys. Rev. Lett. **108**, 269601 (2012); G. Tsekenis, N. Goldenfeld, and K.A. Dahmen, Phys. Rev. Lett. **108**, 269602 (2012).
 - [23] D.M. Dimiduk, C. Woodward, R. LeSar, and M.D. Uchic, Science **312**, 1188 (2006).
 - [24] L. Laurson, and M.J. Alava, Phys. Rev. E **74**, 066106 (2006).
 - [25] C. Reichhardt and C.J. Olson Reichhardt, Phys. Rev. Lett. **103**, 168301 (2009).
 - [26] S. Field, J. Witt, F. Nori, and X.S. Ling, Phys. Rev. Lett. **74**, 1206 (1995).
 - [27] A.C. Marley, M.J. Higgins, and S. Bhattacharya, Phys. Rev. Lett. **74**, 3029 (1995).
 - [28] C.J. Olson, C. Reichhardt, and F. Nori, Phys. Rev. B **56**, 6175 (1997).
 - [29] S. Okuma, Y. Tsugawa, and A. Motohashi, Phys. Rev. B **83**, 012503 (2011).
 - [30] P.D. Ispanovity, I. Groma, G. Györgyi, P. Szabó, and W. Hoffelner, Phys. Rev. Lett. **107**, 085506 (2011).
 - [31] J.P. Hirth and J. Lothe, *Theory of Dislocations* (Wiley, New York, 1982).
 - [32] H. Mughrabi, Mater. Sci. Eng. **85**, 15 (1987).
 - [33] D. Kuhlman-Wilsdorf, Scripta Mater. **34**, 641 (1996).
 - [34] U.F. Kocks, T. Hasegawa, and R.O. Scattergood, Scripta Metal. **14**, 449 (1980).
 - [35] M.G. Stout and A.D. Rollett, Metal. Trans. A **21**, 3201 (1990).
 - [36] Q. Xue, I.J. Beyerlein, and D.J. Alexander, Acta Mater. **55**, 655 (2007).
 - [37] X. Huang, A. Borrego, and W. Pantelon, Mater. Sci. Eng. A **319-321**, 237 (2001).
 - [38] D.A. Hughes and N. Hansen, Acta Mater. **48**, 2985 (2000).
 - [39] F. Dalla Torre, R. Lapovok, J. Sandlin, P.F. Thomson, C.H.J. Davies, and E.V. Pereloma, Acta Mater. **52**, 4819 (2004).
 - [40] F.H. Dalla Torre, E.V. Pereloma, and C.H.J. Davies, Acta Mater. **54**, 1135 (2006).
 - [41] J.C.M. Li, *Electron Microscopy and Strength of Crystals*. (Interscience, New York, 1963).
 - [42] See EPAPS document X.
 - [43] A. Pertsinidis and X.S. Ling, Phys. Rev. Lett. **100**, 028303 (2008).
 - [44] U.F. Kocks, and H. Mecking, Prog. Mater. Sci. **114**, 171 (2003).
 - [45] J.C.M. Li, Acta Metall. **8**, 296 (1960).

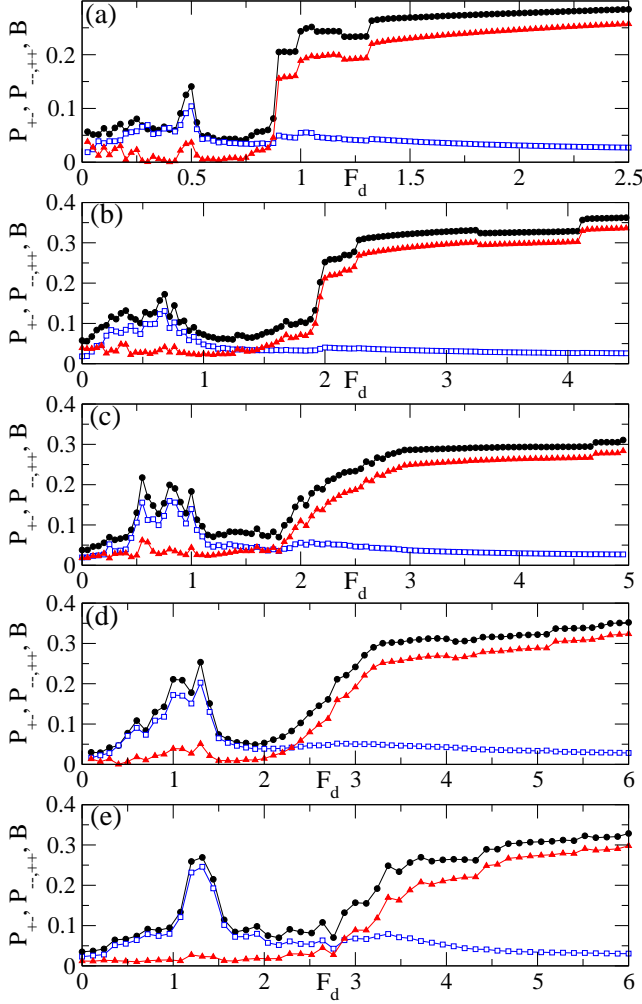


FIG. 1: (Supplemental) P_{+-} (blue squares), the fraction of walls containing dislocations with both positive and negative Burgers vectors, $P_{--,+}$ (black circles), the fraction of walls composed of a single polarity of burgers vectors, and B , the net Burgers vector in the walls, vs F_d for samples with different numbers of dislocations N_D . **a** $N_D = 48$. **b** $N_D = 96$. **c** $N_D = 144$. **d** $N_D = 192$. **e** $N_D = 240$. **f** $N_D = 360$. The same three regimes, pinned, fluctuating, and reordered, occur for all values of N_D , but the location of the regimes shifts to different values of F_d as N_D changes.

SUPPLEMENTARY INFORMATION FOR “DYNAMIC PHASES, PINNING, AND PATTERN FORMATION FOR DRIVEN DISLOCATION ASSEMBLIES”

C. Zhou, C. Reichhardt, C.J. Olson Reichhardt, and
I.J. Beyerlein

Size effects on dynamical transitions: We mea-

sured dynamical reordering curves for samples with different numbers of dislocations N_D . The results in Fig. 2(a) are for a sample with $N_D = 480$. Figure S1 shows

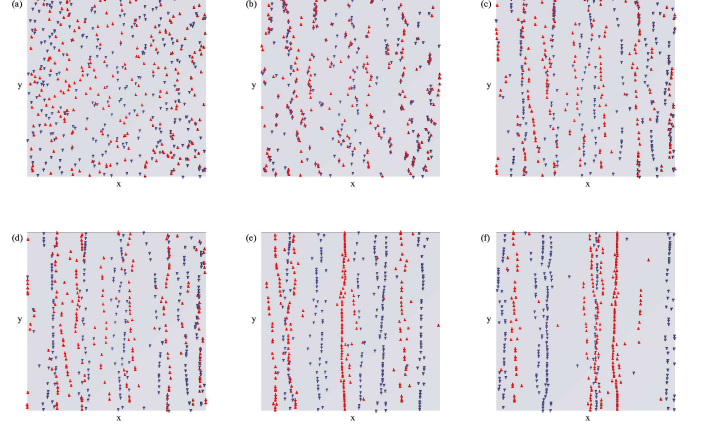


FIG. 2: (Supplemental) The red (blue) crosses are the locations of the dislocations with positive (negative) Burgers vectors in a sample with $N_D = 480$ that has been instantaneously loaded with $F_d = 10$. The time progression of the formation of multiple unipolar walls is illustrated. **a** Initial dislocation configuration. **b** After 1 time unit. **c** After 3 time units. **d** After 5 time units. **e** After 20 time units. **f** After 149 time units.

corresponding plots of P_{+-} , $P_{--,+}$, and B as a function of F_d for samples with $N_D = 48, 96, 144, 192, 240$, and 360 . The three regimes, pinned, fluctuating, and reordered, illustrated in Fig. 2(a) also appear in the smaller samples illustrated in Figure S1, but the transitions between the regimes shift to lower values of F_d as N_D decreases.

Instantaneous loading: In a sample that is instantaneously subjected to a high load, we find a transient disordered phase followed by the formation of multiple lower density unipolar walls instead of the two unipolar walls shown in Fig. 1(g). For the sample with $N_D = 480$, Figure S2 illustrates the time progression of this process when we instantaneously increase F_d to $F_d = 10$.